The Ice-Ocean governor: ice-ocean stress feedback limits Beaufort Gyre spin up

Gianluca Meneghello*[1], John Marshall[1], Jean-Michel Campin[1], Edward Doddridge[1], Mary-Louise Timmermans[2]

[1]Department of Earth, Atmospheric and Planetary Sciences, MIT, Cambridge, Massachusetts, USA

[2]Department of Geology and Geophysics, Yale University, New Haven, Connecticut, USA

*e-mail: gianluca.meneghello@gmail.com

February 24, 2018

Abstract

The Arctic Ocean's Beaufort Gyre is spun up by the prevailing anticyclonic winds forcing sea-ice and ocean motion. A regulator is described that limits spin up and explains the stabilization of the sea-ice covered Beaufort Gyre, even while subject to sustained anticyclonic wind-stress curl. Anticyclonic surface stress due to sea-ice drift drives Ekman downwelling which intensifies the gyre geostrophic flow. The geostrophic flow, in turn, reduces ice-ocean relative speeds and surface stresses: an ice-ocean stress governor. Analytical and numerical modeling is employed to demonstrate the mechanism, contrasting equilibration processes in an ice-covered versus ice-free gyre. Observations are presented and interpreted in terms of the governor mechanism. Our study suggests that continued Arctic sea-ice loss will lead to reduced effectiveness of the governor and change the fundamental internal dynamics of the gyre.

1 Introduction

Anticyclonic winds centered over the Arctic Ocean's Beaufort Gyre (BG) force a lateral Ekman transport in the surface ocean, bringing surface freshwater towards the center of the gyre and driving downwelling. Ekman processes spin up the BG geostrophic circulation and increase its freshwater content [1–5]. Freshwater accumulation, storage and release from the BG, controlled by these wind-driven dynamics, have far-reaching influence on Arctic and global climate [4]. Wind variability alone cannot completely explain the variability in freshwater content [6]: gyre spin up and freshwater increase are complicated by the presence of sea ice cover, which mediates wind forcing on the ocean. Here we show how the dynamic interaction of under-ice geostrophic ocean currents and sea-ice (an *ice-ocean stress governor*) plays a key role in regulating the strength and sign of the ice-ocean stress curl and gyre spin up.

Stress $\boldsymbol{\tau}$ at the ocean surface is a combination of ice-ocean stress $\boldsymbol{\tau}_i$ and air-ocean stress $\boldsymbol{\tau}_a$, each of which may be estimated by a quadratic drag law, weighted by the sea-ice concentration α [7]:

$$\boldsymbol{\tau} = \alpha \underbrace{\rho C_{Di} \left|\boldsymbol{u}_{rel}\right| (\boldsymbol{u}_{rel})}_{\boldsymbol{\tau}_i} + (1-\alpha) \underbrace{\rho_a C_{Da} \left|\boldsymbol{u}_a\right| (\boldsymbol{u}_a)}_{\boldsymbol{\tau}_a} . \quad (1)$$

C_{Di} and C_{Da} are drag coefficients for the ice-ocean and air-ocean stress respectively, ρ is water density, and ρ_a is air density. In the computation of $\boldsymbol{\tau}_a$, the surface ocean velocity, of a few cm s^{-1}, is considered negligible with respect to a 10-m wind velocity $\boldsymbol{u}_a$ of a few m s^{-1}.

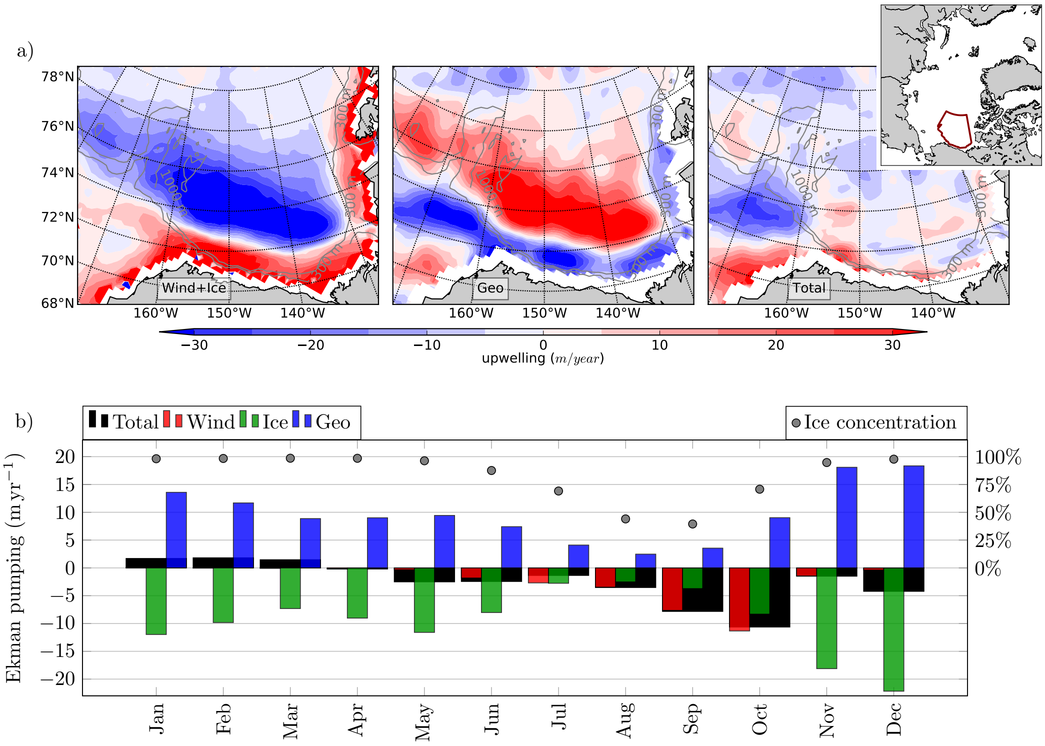

Figure 1. Ekman pumping climatology. (a) Mean Ekman pumping over 2003-2014; negative (blue) indicates downwelling, positive (red) upwelling. Left: downwelling estimates locally exceed 30 m yr^{-1} if the geostrophic current is neglected; center: inclusion of the geostrophic current results in an upwelling effect, largely compensating the ice-driven downwelling; right: the actual Ekman pumping, the sum of the previous two panels, yields only moderate downwelling together with patches of upwelling. The BG Region (BGR) is marked by a red line in the inset. (b) Monthly Ekman pumping climatology over the BGR and its partitioned contributions, where negative indicates downwelling. Black bars show total Ekman pumping, equivalent to the right panel in a). Red and green bars show pumping induced by winds driving ice-free regions, and pumping under ice for zero geostrophic flow; their sum is equivalent to the left panel in a). Blue bars show pumping induced by geostrophic currents flowing under the sea ice, equivalent to the central panel in a). Blue and green bars largely balance each another, and exactly balance if $\boldsymbol{u}_{rel}$=0. Grey dots represent ice concentration.

On the other hand, surface ocean velocity cannot be neglected in the estimation of $\boldsymbol{\tau}_i$. The ice-ocean relative velocity $\boldsymbol{u}_{rel}$ is expressed as the difference between the ice velocity $\boldsymbol{u}_i$ and the surface ocean velocity, taken to be the sum of geostrophic $\boldsymbol{u}_g$ and ageostrophic (Ekman) $\boldsymbol{u}_e$ components. That is $\boldsymbol{u}_{rel} = \boldsymbol{u}_i - (\boldsymbol{u}_g + \boldsymbol{u}_e)$.

Observations allow estimates of $\boldsymbol{\tau}$, which may be used to produce climatologies of the Ekman pumping rate $w_{Ek} = \nabla \times (\frac{\tau}{\rho f})$ in the BG Region, BGR (Figure 1), where ρ is a reference water density and f is the Coriolis parameter. The intensity of the ocean surface currents plays a central role in modulating the Ekman pumping [8–11]. The strong wind- and ice-induced downwelling locally exceeds $30\,\mathrm{m\,yr^{-1}}$ if the geostrophic current is neglected (Figure 1a, blue region in the left panel). This is largely compensated by the upwelling effect of the surface current flowing against the ice (red region in the central panel), acting as a negative feedback and turning off the downwelling. That is, the governor drives the system towards $\boldsymbol{u}_{rel} = 0$. Consequently the Ekman pumping is strongly reduced (right panel). A monthly climatology of Ekman pumping and its components averaged over the BGR (Figure 1b) shows how the total Ekman pumping is reduced by the geostrophic current, and even reversed during the months of January, February and March [8].

We demonstrate here how the governor can be a mechanism for the equilibration of freshwater content in the gyre. For example, should the anticyclonic ice stress curl intensify, the geostrophic flow of the gyre will strengthen until the governor "kicks in" and reduces the surface stress. This is a distinct alternative to the eddy-equilibration mechanism first proposed for the southern ocean [12, 13], and more recently extended to the BG [9, 14–18]. In the next section, we analyze the response of an idealized gyre under two different limit-case scenarios: i) an ice-driven gyre (α=1, in which forcing depends purely on gradients of $\boldsymbol{\tau} = \boldsymbol{\tau}_i$) and ii) an ice free, wind-driven gyre (α=0, in which forcing depends purely on gradients of $\boldsymbol{\tau} = \boldsymbol{\tau}_a$). We then conclude by discussing observations of Ekman pumping and dynamic topography in the BG over the last decade or so, in terms of the ice governor mechanism. Finally we speculate on what might happen as the governor becomes less effective in a warming world and an increasingly ice free Arctic Ocean.

2 The ice-ocean stress governor

We run numerical experiments employing a high resolution idealized model of the BG based on the MIT General Circulation Model [19, 20] designed to capture both mesoscale eddy processes and the ice-ocean governor mechanism. Simulations begin with a uniformly-stratified ocean at rest in which freshwater is pumped down through the action of either a wind-driven or an ice-driven surface stress. The ocean is spun up via a steady axisymmetric, anticyclonic, wind/ice field (zero speed at the center of the domain, reaching a maximum at a radius 300 km), broadly consistent with observations [8]. Wind and ice velocity magnitudes are chosen to produce the same surface stress $\boldsymbol{\tau}_0$ when the ocean is at rest. The stress remains constant in the ice-free case α=0, but evolves and, in fact, diminishes in time in the ice-driven case α=1 as the surface currents spin up to match the ice speed. Five experiments are run for each scenario, varying ice and wind velocities. Additional model details are provided in the Supplementary material. We diagnose the gyre response by computing the maximum depth anomaly h of the $S = 31$ isohaline.

2.1 Ice-driven gyre ($\alpha = 1$): stress-equilibrated

We begin by describing the evolution of a typical ice-covered simulation in which the ice governor operates (Figure 2a, left panel and Figure 2b, thick blue line). Ice-covered experiments have imposed anticyclonic ice drift with a range of maximum speeds broadly in agreement with observations [8]; our example simulation has an ice-speed maximum of $8\,\mathrm{cm\,s^{-1}}$, corresponding to a surface stress $\tau_0 = 0.04\,\mathrm{N\,m^{-2}}$. Initially, the ocean is at rest and the applied surface stress gives rise to an Ekman pumping of order $w_{Ek} \approx \tau_0/(\rho f R) \approx 30\,\mathrm{m\,yr^{-1}}$, where $R \approx 300\,\mathrm{km}$ is the radius of the gyre and $f = 1.45 \times 10^{-4}\,\mathrm{s^{-1}}$. As time progresses, a geostrophic current is spun up; by year 10, the ocean surface speed is approximately equal to the ice-drift speed (Figure 2a, top row). After 10-15 years h stabilizes at a depth of around 50 m (Figure 2b, thick blue line). A relatively mild baroclinic instability develops around year 20, but the ice-ocean stress governor is sufficiently efficient in the ice-covered scenario that baroclinic instability does not play any appreciable role in gyre equilibration. We remark that the time at which baroclinic instability develops depends on the gyre depth, and finally on the ice velocity.

The isopycnal depth anomaly h increases at a rate proportional to w_{Ek}, which is proportional to the curl of the surface stress $\boldsymbol{\tau}_i$ so that we may write

$$\frac{dh}{dt} = \frac{\gamma}{\rho f}\frac{\tau_i}{R}, \tag{2}$$

where γ is a dimensionless constant that depends on the spatial distribution of the Ekman pumping and the geometry of the isopycnal slope.

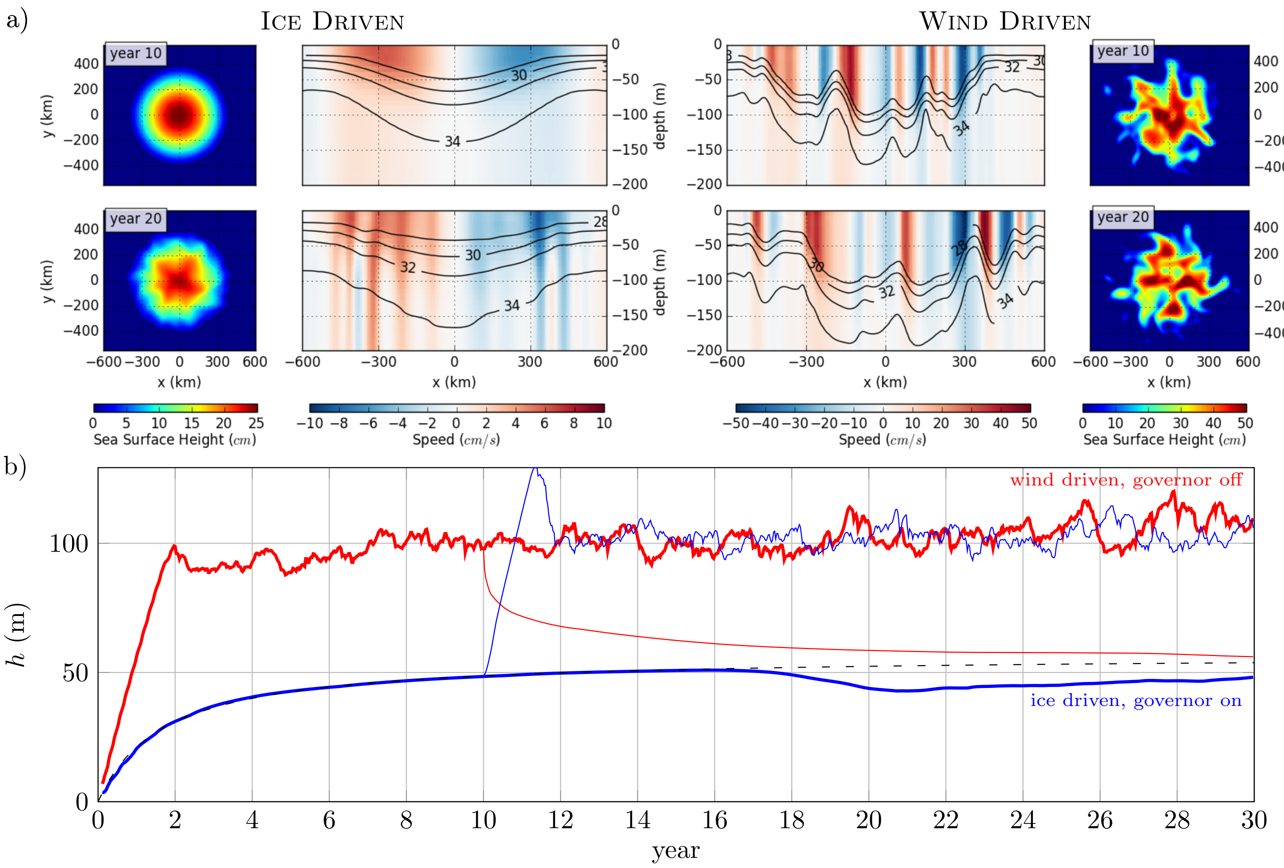

Figure 2. (a) Instantaneous sea surface height (exterior panels), vertical section of salinity (central panels, black contours) and speed (central panels, color) at years 10 (top row) and 20 (bottom row) for the ice-driven (α=1 and $u_i = 8\,\mathrm{cm\,s^{-1}}$, left) and the wind-driven (α=0 and $u_a = 4.8\,\mathrm{m\,s^{-1}}$, right) scenarios. Note the different ranges (color scales) between the two cases. Only the top 200 m of the 800 m domain depth are shown in the central panels. (b) Depth anomaly of the 31 isohaline for the ice driven $\alpha = 1$ (blue) and wind driven $\alpha = 0$ (red) scenario. For α=1, Ekman pumping spins up the gyre until the surface ocean speed ($\boldsymbol{u}_g + \boldsymbol{u}_e$) approaches the ice-drift speed (such that $\boldsymbol{u}_{rel}$ approaches 0), thus turning off the ice-ocean stress driving spin up. Evidence of weak baroclinic instability is visible in the later stages of the evolution (around 20 years). For α=0, the gyre inflates at a rate proportional to the Ekman pumping until it reaches a quasi-equilibrium in which Ekman pumping is balanced by baroclinic instability and lateral eddy fluxes out of the gyre. Thin lines in panel b) show the transition between an ice-covered and an ice-free state (blue), and vice versa (red). The dashed black line is a fit of equation (6), and is almost indistinguishable from the numerical solution before year 16.

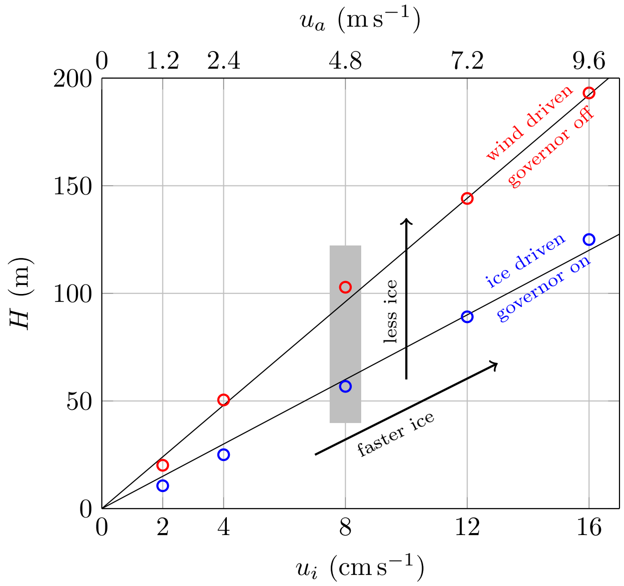

Figure 3. Asymptotic isopycnal depths H for 5 different model runs each of the wind-driven (H_K, red) and ice-driven (H_τ, blue) scenarios, as a function of the wind and ice velocity respectively. The gray area marks the example cases shown in Figure 2. Arrows show two possible mechanisms for altering the depth of the gyre: an increase of the ice speed — faster ice — and the turning off of the ice-ocean governor due to a reduced ice cover — less ice.

In order to obtain an analytical solution which enables us to identify controlling parameters, we make the following approximations. First, the Ekman velocity u_e may be reasonably neglected in estimating τ_i. This velocity scales as $u_e \sim \tau_i/(\rho f D_e)$, where $D_e \approx 20\,\mathrm{m}$, the Ekman layer depth. It can be shown that when τ_i scales as the square of $\left[(u_i - u_g) - u_e\right]$ then $u_e/(u_i - u_g)$ does not exceed 0.2 for the range of u_i considered here. Therefore it is a reasonable approximation to neglect u_e in the analytical model so that τ_i is only a function of u_i and u_g. Second, we suppose the bottom current to be negligible so that the magnitude of the surface geostrophic velocity may be estimated by the thermal wind relationship as follows

$$u_g \sim \frac{g'}{f}\frac{h}{R}, \tag{3}$$

where $g' = g\Delta\rho/\rho$ is the reduced gravity and $\Delta\rho$ is the vertical density difference between the top and bottom of the model domain. The close agreement between theory and simulation, reported below, also attests to the validity of these approximations.

With equation (3) and (1), equation (2) may be expressed as

$$\frac{dh}{dt} = \frac{H_\tau}{T_\tau}\left(1 - \frac{h}{H_\tau}\right)^2, \tag{4}$$

where

$$H_\tau = \frac{f}{g'} R u_i \qquad T_\tau = \frac{(fR)^2}{\gamma g' C_{Di} u_i} \tag{5}$$

are ice-stress-equilibrated length and time scales, respectively. The scale H_τ is the stress-equilibrated steady-state isopycnal depth (i.e., $dh/dt = 0$ when $h = H_\tau$). It can be seen from equation (3) that $h = H_\tau$ is equivalent to $u_g = u_i$ (i.e., $u_{rel} = 0$). In this limit the gyre has been equilibrated by the ice-ocean stress governor. Equation (4), with $h(t = 0) = 0$, has solution

$$h = H_\tau \left(\frac{t}{t + T_\tau} \right). \tag{6}$$

Values of H_τ are obtained by fitting equation (6) to each simulation, and show a linear dependence on u_i as expected from equation (5) (Figure 3, blue circles).

2.2 Wind-driven gyre (α=0): eddy-equilibrated

The reference wind driven experiment (Figure 2a, right, and Figure 2b, thick red line) has an imposed anticyclonic wind-speed maximum of $4.8\,\mathrm{m\,s^{-1}}$, corresponding to a surface stress of $\tau_a = 0.04\,\mathrm{N\,m^{-2}}$, equivalent to the initial stress in the ice-driven scenario. Initially, the depth of the gyre (diagnosed by h) increases linearly at a rate proportional to the vertical Ekman velocity which scales as $w_{Ek} \sim \tau_a/(\rho f R) \approx 30\,\mathrm{m\,yr^{-1}}$ (Figure 2b, thick red line). The linear increase in h proceeds until baroclinic instability develops. By year 2 of the simulation, $h \approx 100$ m, or twice the asymptotic isopycnal depth anomaly of the ice-driven scenario. Baroclinic instability arrests the deepening with eddy fluxes transporting freshwater laterally out of the gyre (Figure 2a, left). The gyre reaches a quasi-steady equilibrium characterized by an active eddy field, and a balance between Ekman downwelling and eddy fluxes[9, 16, 17].

The steady equilibrium state of the gyre can be described as a balance between the mean (Eulerian) overturning streamfunction (proportional to surface wind stress), and the eddy overturning streamfunction [13, 21, 22]. This *vanishing residual-mean* circulation framework[9] yields the following scaling for the equilibrated value of h:

$$H_K \sim \frac{R}{\rho f K} \tau_a = \frac{R}{\rho f K} \rho_a C_{Da} u_a^2 = u_a R \sqrt{\frac{\rho_a C_{Da}}{\rho f \kappa}}, \tag{7}$$

where K is eddy diffusivity and the subscript K implies eddy equilibrated. The final equality assumes a linear relationship between eddy diffusivity and isopycnal slope, $K = \kappa H_K/R$ (for some constant κ). The linear relationship between u_a and equilibrated isopycnal depth H_K

implied by equation (7) is clear over the range of imposed u_a in the five wind-driven simulations (Figure 3, red circles).

Finally we carried out two experiments to examine the effect of a sudden transition between an ice-covered and an ice-free gyre. The eddying, deeper halocline transitions rapidly to a non-eddying solution when the governor is turned on (Figure 2b, thin red line), and the shallower, non-eddying solution transitions to an eddying solution when the governor is turned off (Figure 2b, thin blue line).

3 Implications of the ice-governor

We have analyzed and compared two different mechanisms governing the equilibration of the Beaufort Gyre. In the wind driven scenario in the absence of ice, the depth of the gyre is governed by the balance between Ekman pumping and a vigorous eddy field releasing freshwater by baroclinic instability. This has been previously hypothesized to play a central role in gyre equilibration [9, 16]. Here we have shown that another fundamental mechanism is at play in the presence of ice, namely the ice-ocean stress governor, a negative feedback between the ice-mediated Ekman pumping and the surface geostrophic currents of the gyre. By examining the limiting cases ($\alpha = 1$ and $\alpha = 0$), we have demonstrated how the spin up of the gyre, and its isopycnal depth anomaly, can be regulated by the interaction between the sea-ice and the surface geostrophic current flowing at comparable speeds.

Evidence of the role of the ice-ocean governor over the observational period can be seen by comparing the Ekman pumping climatology and Dynamic Ocean Topography (DOT) [23], Figure 4. Over the record upwelling driven by the geostrophic flow approximately balances downwelling (evidence of the governor in action), with the exception of two notable years: 2007 and 2012. In 2007, strong anticyclonic wind forcing resulted in a strong increase of the DOT anomaly. The gyre consequently sped up, with stronger geostrophic currents against the sea ice inducing upwelling. In 2012, cyclonic winds [25] resulted in a net total upwelling and a reduction in the gyre DOT, with the system moving back towards the previous equilibrium in the following years. We remark that the 2012 ice component is still downwelling favorable: it is the presence of the geostrophic current that drives a strong upwelling in the ice covered part of the gyre; a similar but less marked effect is present in 2009, 2010, 2011 and 2014. Clearly the ice-ocean governor is a strong process relaxing the system back to an equilibrium despite variable upwelling/downwelling signals imposed by the wind.

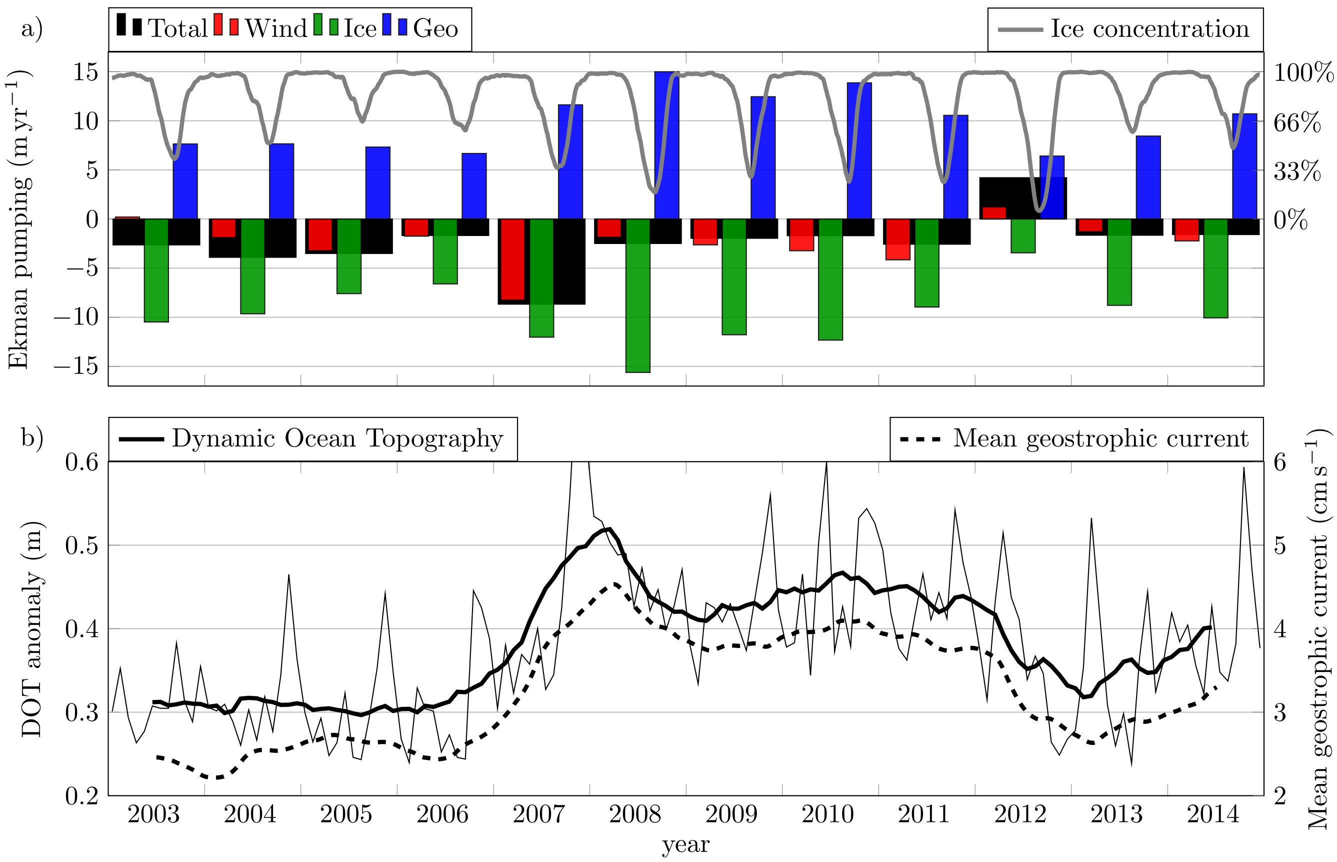

Figure 4. a) Yearly climatology of Ekman pumping (black bars) and its wind (red), ice with zero geostrophic current (green), and geostrophic current components (blue); mean ice concentration is shown by the gray thick line. b) Dynamic Ocean Topography[23] (DOT) anomaly over the BGR (solid thin line), its yearly running mean (solid thick line), and yearly running mean of mean geostrophic current [24] (thick dashed line).

This same equilibrium can be disrupted in two ways, as summarized by the arrows in Figure 3: a change in the wind or ice velocity, as already suggested by previous authors [6], or a change in the effectiveness of the ice-ocean governor, as suggested in the present work. The pronounced seasonal cycle in the BG gives rise to wind-driven downwelling in summer/fall (when sea-ice extent is smallest and ice is most mobile) and ice-ocean stress induced upwelling during the winter months, when the ice-ocean governor is most effective due to the extensive sea-ice cover (Figure 1b). This suggests the potential for an important shift in BG dynamics under projected continued summer sea-ice decline in the coming years and decades. Increased summer Ekman downwelling will result in a deeper gyre and faster geostrophic current, while the faster geostrophic current will result in strong upwelling during the ice-covered winter: depending on gyre response timescales, a stronger seasonal cycle in isopycnal depth is to be expected due to the alternation of summers characterized by very mobile ice and ice-covered winters. This will in turn impact the dynamics of the halocline insulating the ice-cover from the warmer waters at depth, and hence on the persistence of the ice-cover itself.

Acknowledgements

The authors thankfully acknowledge support from NSF Polar Programs, both Arctic and Antarctic.

Author contributions

All authors contributes equally to this study.

Additional information

The authors declare no competing financial interests.

References

1. Proshutinsky, A. Y. & Johnson, M. A. Two circulation regimes of the wind-driven Arctic Ocean. *Journal of Geophysical Research: Oceans* **102,** 12493–12514 (1997).
2. Proshutinsky, A., Bourke, R. H. & McLaughlin, F. A. The role of the Beaufort Gyre in Arctic climate variability: Seasonal to decadal climate scales. *Geophysical Research Letters* **29,** 15–1 (2002).

3. Proshutinsky, A. *et al.* Beaufort Gyre freshwater reservoir : State and variability from observations. *Journal of Geophysical Research* **114,** 1–25 (2009).

4. Proshutinsky, A., Dukhovskoy, D., Timmermans, M.-l., Krishfield, R. & Bamber, J. L. Arctic circulation regimes. *Philosophical transactions. Series A, Mathematical, physical, and engineering sciences* **373,** 20140160 (2015).

5. Timmermans, M. L. *et al.* Surface freshening in the Arctic Ocean's Eurasian Basin: An apparent consequence of recent change in the wind-driven circulation. *Journal of Geophysical Research: Oceans* **116** (2011).

6. Giles, K. A., Laxon, S. W., Ridout, A. L., Wingham, D. J. & Bacon, S. Western Arctic Ocean freshwater storage increased by wind-driven spin-up of the Beaufort Gyre. *Nature Geoscience* **5,** 194–197 (2012).

7. Yang, J. Seasonal and interannual variability of downwelling in the Beaufort Sea. *J Geophys Res* **114,** C00A14 (2009).

8. Meneghello, G., Marshall, J., Timmermans, M. L. & Scott, J. Observations of seasonal upwelling and downwelling in the Beaufort Sea mediated by sea ice. *J. Phys. Oceanogr.* **in press** (2018).

9. Meneghello, G., Marshall, J., Cole, S. T. & Timmermans, M.-L. Observational inferences of lateral eddy diffusivity in the halocline of the Beaufort Gyre. *Geophysical Research Letters* **44** (Nov. 2017).

10. Zhong, W., Steele, M., Zhang, J. & Zhao, J. Greater Role of Geostrophic Currents in Ekman Dynamics in the Western Arctic Ocean as a Mechanism for Beaufort Gyre Stabilization. *Journal of Geophysical Research: Oceans* (Jan. 2018).

11. Dewey, S. *et al.* Arctic Ice-Ocean Coupling and Gyre Equilibration Observed With Remote Sensing. *Geophysical Research Letters* (Feb. 2018).

12. Karsten, R., Jones, H. & Marshall, J. The Role of Eddy Transfer in Setting the Stratification and Transport of a Circumpolar Current. *Journal of Physical Oceanography* **32,** 39–54 (2002).

13. Marshall, J. & Radko, T. Residual-Mean Solutions for the Antarctic Circumpolar Current and Its Associated Overturning Circulation. *Journal of Physical Oceanography* **33,** 2341–2354 (2003).

14. Davis, P. E. D., Lique, C. & Johnson, H. L. On the link between arctic sea ice decline and the freshwater content of the beaufort gyre: Insights from a simple process model. *Journal of Climate* **27,** 8170–8184 (2014).

15. Lique, C., Johnson, H. L. & Davis, P. E. D. On the Interplay between the Circulation in the Surface and the Intermediate Layers of the Arctic Ocean. *Journal of Physical Oceanography* **45,** 1393–1409 (2015).

16. Manucharyan, G. E., Spall, M. A. & Thompson, A. F. A Theory of the Wind-Driven Beaufort Gyre Variability. *Journal of Physical Oceanography,* 3263–3278 (2016).

17. Manucharyan, G. E. & Spall, M. A. Wind-driven freshwater buildup and release in the Beaufort Gyre constrained by mesoscale eddies. *Geophysical Research Letters* **43,** 273–282 (2016).

18. Yang, J., Proshutinsky, A. & Lin, X. Dynamics of an idealized Beaufort Gyre: 1. the effect of a small beta and lack of western boundaries. *Journal of Geophysical Research: Oceans* **121,** 1249–1261 (2016).

19. Marshall, J., Adcroft, A., Hill, C., Perelman, L. & Heisey, C. A finite-volume, incompressible Navier Stokes model for studies of the ocean on parallel computers. *Journal of Geophysical Research: Oceans* **102,** 5753–5766 (1997).

20. Marshall, J., Hill, C., Perelman, L. & Adcroft, A. *Hydrostatic, quasi-hydrostatic, and nonhydrostatic ocean modeling* 1997.

21. Andrews, D. G. & McIntyre, M. E. Planetary Waves in Horizontal and Vertical Shear: The Generalized Eliassen-Palm Relation and the Mean Zonal Acceleration. *Journal of the Atmospheric Sciences* **33,** 2031–2048 (1976).

22. Plumb, R. A. & Ferrari, R. Transformed Eulerian-Mean Theory. Part I: Nonquasigeostrophic Theory for Eddies on a Zonal-Mean Flow. *Journal of Physical Oceanography* **35,** 165–174 (2005).

23. Armitage, T. W. K. *et al.* Arctic sea surface height variability and change from satellite radar altimetry and GRACE, 2003-2014. *Journal of Geophysical Research: Oceans* **121,** 4303–4322 (2016).

24. Armitage, T. W. K. *et al.* Arctic Ocean geostrophic circulation 2003-2014. *The Cryosphere Discussions* **2017,** 1–32 (2017).

25. Simmonds, I. & Rudeva, I. The great Arctic cyclone of August 2012. *Geophysical Research Letters* **39,** 1–6 (2012).

26. Nurser, A. J. G. & Bacon, S. The rossby radius in the arctic ocean. *Ocean Science* **10,** 967–975 (2014).

SUPPLEMENTARY INFORMATION

A: Numerical model details

A configuration of the MIT General Circulation Model [19, 20] is employed for the numerical experiments described here. The domain is a 1200x1200 km by 800 m box with 4 km horizontal resolution and 40 levels in the vertical, most of them near the surface to resolve the developing halocline. The Rossby deformation radius in the Beaufort Gyre region being $\approx$ 15 km [26], the model can be considered eddy resolving and is thus able to reproduce both the eddy and the ice-ocean governor processes.

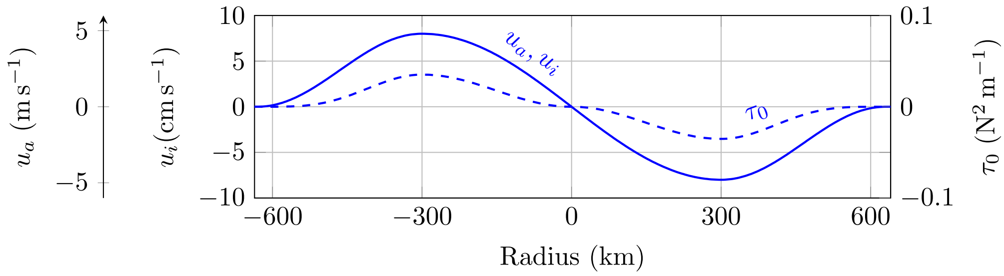

Figure A.1. Forcing profile for the wind and ice driven model experiments (solid line) and equivalent surface stress (dashed line). In the ice driven case, the surface stress is for the ocean at rest.

All simulations begin with the ocean at rest, and salinity linearly increasing from 34 psu at the surface to 35 psu at 800 m; density is considered to be a function of salinity only, effectively the case in the BG, and a linear equation of state is used. The ocean is spun up by time-invariant axisymmetric, anticyclonic, wind and ice velocity profiles shown in Figure A.1, and surface stress is computed from velocity using the equivalent of equation (1) with $\alpha = 0$ or 1 over the entire domain. The stress remains constant in the wind-driven scenario $\alpha = 0$, but is reduced by the increasing ocean surface velocity in the ice-driven scenario $\alpha = 1$. Surface salinity is relaxed to a target value of 27 psu during the spin up process, and bottom salinity to 35 psu, consistent with BG observations. The wind and ice velocities are within the range of observed values [8], and are chosen to produce the same surface stress when the ocean is at rest. $f-$plane dynamics are considered with Coriolis parameter $f = 1.45 \times 10^{-4}\,\mathrm{s}^{-1}$, and a vertical diffusion coefficient of $1 \times 10^{-3}\,\mathrm{m}^2\,\mathrm{s}^{-1}$ is used. Isopycnal depth anomaly is computed as the difference between the maximum and the minimum depth of the 31 psu isohaline over the entire domain.